

Electronic Structure and Bulk Spin Valve Behavior in $\text{Ca}_3\text{Ru}_2\text{O}_7$

D.J. Singh¹ and S. Auluck²

¹Condensed Matter Sciences Division, Oak Ridge National Laboratory, Oak Ridge, TN 37831-6032, USA

²Physics Department, Indian Institute of Technology, Roorkee (Uttaranchal) 247667, India

We report density functional calculations of the magnetic properties and Fermiology of $\text{Ca}_3\text{Ru}_2\text{O}_7$. The ground state consists of ferromagnetic bilayers, stacked antiferromagnetically. The bilayers are almost but not exactly half-metallic. In the ferromagnetic state opposite spin polarizations are found for in-plane and out-of-plane transport. Relatively high out of plane conductivity is found for the majority spin, which is relatively weakly conductive in-plane. In the ground state in-plane quantities are essentially the same, but the out of plane transport is strongly reduced.

The perovskite based ruthenates, $D_{1+n}\text{Ru}_n\text{O}_{3n+1}$, $D=\text{Sr,Ca}$ show a remarkable range of electronic and magnetic properties, even though they are all based on Ru^{4+} in octahedral environments with corner sharing topologies. This includes robust itinerant ferromagnetism (SrRuO_3)^{1,2}, paramagnetic “bad” metals (CaRuO_3)³, unconventional superconductivity (Sr_2RuO_4)⁴, an anti-ferromagnetic (AFM) Mott insulator (Ca_2RuO_4)⁵, and metamagnetic quantum critical behavior ($\text{Sr}_3\text{Ru}_2\text{O}_7$)⁶. This reflects exceptionally strong dependence of electronic and magnetic properties on lattice degrees of freedom, also seen in band structure studies^{7,8,9,10}.

The bilayer $n=2$ compounds are of particular interest due to their borderline properties. $\text{Sr}_3\text{Ru}_2\text{O}_7$ bridges the metallic ferromagnetic (FM) $n=\infty$ compound SrRuO_3 and the paramagnetic Fermi liquid Sr_2RuO_4 and has a metamagnetic quantum critical point⁶ associated with borderline metallic ferromagnetism. $\text{Ca}_3\text{Ru}_2\text{O}_7$ is intermediate between the bad metal CaRuO_3 and the Mott insulator Ca_2RuO_4 , and so may be a useful window into the physics of clean materials near a metal insulator transition. Signatures of the borderline physics include strong sensitivity of measured properties to minor sample variations, observation of metallic like properties such as quantum oscillations and finite linear specific heat coefficient in non-conducting material, a large lattice anomaly at the magnetic ordering temperature, and low field metamagnetic transitions with strong transport signatures^{11,12,13,14,15,16,17,18,19,20,21}.

Here, we report detailed electronic structure calculations for $\text{Ca}_3\text{Ru}_2\text{O}_7$. These give insight into a number of key observations – magnetic structure, lattice coupling, and transport. They were done in the local spin density approximation (LSDA) using the general potential linearized augmented planewave (LAPW) method with local orbitals^{22,23}. We used the experimental low temperature (8K) non-centrosymmetric $Bb_{21}m$ crystal structure²¹. This is a centered structure, with two formula units, and a $c(2\times 2)$ in-plane cell doubling due to octahedral tilts and rotation. The strong octahedral tilting differentiates this compound from $\text{Sr}_3\text{Ru}_2\text{O}_7$. Significantly, if insulating, this non-centrosymmetric space-group would have a ferroelectric polarization along b . This would be of interest in the context of magnetoelectrics if a related well insulating, but magnetic, ma-

terial can be made. The calculations were highly converged with respect to basis set and zone samplings^{24,25}. Approximately 2650 LAPW basis functions were used, and twice that number for the doubled cell. The Fermi surfaces are based on an interpolation from 494 first principles points in the irreducible wedge of the zone, except for the doubled AFM cell, where 194 points were used.

$\text{Ca}_3\text{Ru}_2\text{O}_7$ shows an AFM ordering at $T_N=56\text{K}$ and a transition from a metal to a low temperature poorly conductive or insulating phase at 48K .¹¹ Metamagnetic transitions to an effectively ferromagnetic phase, with large changes in conductance occur at relatively low field, depending on the field direction while magnetization measurements imply that the RuO_2 layers themselves are ferromagnetically ordered, with an AFM stacking¹⁶. Three possible AFM stackings have been suggested – ferromagnetic bi-layers stacked antiferromagnetically, or bi-layers that are internally antiferromagnetically aligned, stacked either in a FM or an AFM fashion, i.e. (1) $-UU - DD - UU -$, (2) $-UD - UD - UD -$ or (3) $-UD - DU - UD -$ along c . Recent neutron scattering experiments favor ordering (1) over ordering (2), based on observation of half order diffraction peaks.²¹ Considering the layered crystal structure and highly 2D electronic structure (see below), magnetic interactions within a bilayer must be very much stronger than inter-bilayer couplings. Calculated energetics are given in Table I. The non-spin-polarized state (P) is unstable against ferromagnetism by 70 meV/f.u., but state (2), is favored over P by only 19 meV/f.u. In plane antiferromagnetism is also disfavored relative to ferromagnetism. Thus AFM in the bilayers is strongly disfavored, and the ground state must be (1) and not (3). In fact, (1), consisting of ferromagnetic bi-layers stacked antiferromagnetically is an additional 5 meV/f.u. lower than the FM state, so the inter-bilayer coupling is weakly AFM. We did structural relaxations of all atomic positions in the $Bb_{21}m$ cell. This yields an energy gain of only 16 meV (per 12 atom formula unit) for FM ordering, supporting the experimental crystal structure, and a larger 27 meV for the non-spin-polarized case, the difference implying significant magnetoelastic coupling. For magnetism with itinerant character, this can provide an explanation of the structural anomalies at the ordering temperature.

Since the inter-bilayer coupling is weak, it is useful to

TABLE I: Calculated magnetic energies. AF1 and AF2 are FM layers stacked -UU-DD-UU- and -UD-UD-UD-, respectively. AFP is in-plane c(2x2) AFM.

ordering	P	FM	AFP	AF1	AF2
E(meV/f.u.)	0	-72	-52	-77	-19

start with the FM state. The calculations show that the mechanism of moment formation and the major sheets of Fermi surface are essentially the same as in the AFM ground state, as are the density of states and in-plane Fermi velocities. However, for the AFM case, the majority and minority spin lie on top of each other due to the alternating spin up and spin down bi-layers.

The spin magnetization with FM ordering is $1.934 \mu_B/\text{Ru}$, of which only $1.23 \mu_B$ is within the Ru LAPW sphere (radius $2.05 a_0$). The remaining $\sim 1/3$ is O in character, comparable to other FM ruthenates^{8,9}. The origin is the strong Ru-O hybridization in these $4d$ compounds, combined with Hund's coupling on O. The electronic density of states (DOS) and projections onto the Ru and O LAPW spheres are shown in Figs. 1 and 2. The optical spectrum is in Fig. 3 and the Fermi surface in Fig. 4. The low energy part of the optical spectrum below ~ 1.5 eV, derives from d - d transitions, while the in-plane peaks at ~ 1.9 eV and ~ 2.5 eV are respectively of majority and minority spin charge transfer p - d character. There is little in-plane anisotropy except at low energy (not shown). Comparison with experiment would be useful in testing the LSDA electronic structure.

Moment formation via an itinerant Stoner instability depending on Ru-O hybridization, similar to SrRuO_3 is clearly seen^{7,8}. Thus the O polarization plays a key role. The importance of the Hund's coupling on O is also evident from the exchange splitting of the O bands as seen in the DOS. The spin moments within the O LAPW spheres (radius $1.65 a_0$) are $0.08 \mu_B$ (apical O), $0.13 \mu_B$ and $0.14 \mu_B$ (two inequivalent in-plane O) and $0.21 \mu_B$ (interlayer bridging O). These are reflected in the various O contributions to the DOS near E_F (Fig. 2). The large bridging O contribution, which also reflects the bonding of the bi-layer units, explains the strong interlayer FM coupling.

Our results and the experimental observation of relatively low field metamagnetism show that the basic magnetic structure is ferromagnetic bilayers, with a very weak inter-bilayer AFM coupling. To understand the electronic structure we begin with the FM bilayers.

Within an ionic model, each Ru has 4 t_{2g} electrons, which partially fill the t_{2g} manifold. Because of band narrowing due to the octahedral tilts and rotation in $\text{Ca}_3\text{Ru}_2\text{O}_7$, this manifold is separated from the higher lying e_g manifold by a gap. If fully polarized, this would yield a spin moment of $2 \mu_B/\text{Ru}$, close to but larger than what we find. The FM DOS shows that the bilayers are almost, but not exactly half metallic. This is similar to the colossal magnetoresistive (CMR) manganites

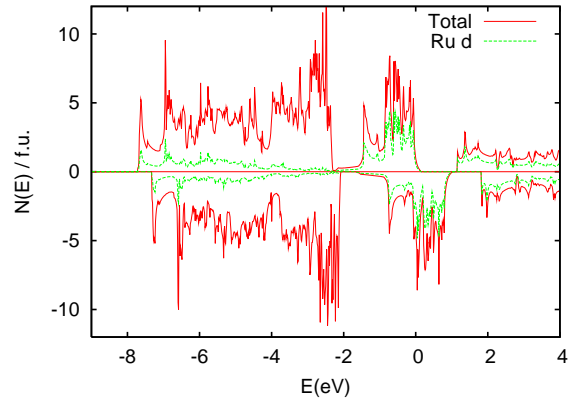


FIG. 1: (color online) Electronic density of states and projection onto the Ru LAPW spheres, radius $2.05 a_0$) of FM $\text{Ca}_3\text{Ru}_2\text{O}_7$ on a per formula unit basis. Majority spin is shown above the axis, and minority below.

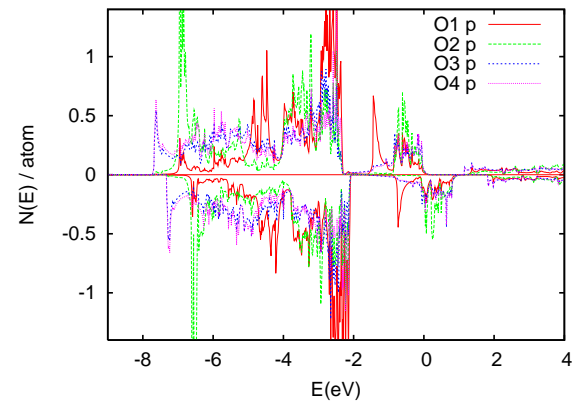


FIG. 2: (color online) Density of states projection onto the O LAPW spheres (radius $1.65 a_0$) on a per atom basis. O1 is the apical O in the CaO rocksalt layers, O2 is the bridging apical O joining the RuO_2 bilayers and O3 and O4 are the plane O in the RuO_2 layers.

such as $(\text{La},\text{Ca})\text{MnO}_3$ ^{26,27}. In those materials, there is a finite density of states in both spin channels, but E_F falls near the minority spin band edge, and those states are Anderson localized. In FM $\text{Ca}_3\text{Ru}_2\text{O}_7$, E_F falls very near the majority spin band edge. However, because it is a clean material, with no alloy scattering, there is no mechanism for Anderson localization at low temperature. Thus, in contrast to the CMR materials, as the temperature is lowered in FM $\text{Ca}_3\text{Ru}_2\text{O}_7$ the majority spin channel will cross-over from localized to metallic, yielding an anisotropic partially spin polarized metal.

In a layered structure, the t_{2g} manifold derives from two sets of bands, d_{xy} which is 2D, and d_{xz} and d_{yz} , which are 1D. For a bilayer, these split into symmetric and antisymmetric combinations due to interlayer hopping. Since the d_{xy} is directed in-plane, its interlayer

TABLE II: Fermi surface parameters of $\text{Ca}_3\text{Ru}_2\text{O}_7$ for the P, FM and AFM ground state AF1. $N(E_F)$ is given in eV^{-1} per spin per f.u. Fermi velocities, $\langle v_i^2 \rangle^{1/2}$ are in cm/s.

	$N(E_F)$	v_a	v_b	v_c
P	5.23	0.78×10^7	0.71×10^7	0.23×10^7
F(majority)	0.95	0.64×10^7	0.71×10^7	0.58×10^7
F(minority)	4.41	1.17×10^7	1.48×10^7	0.22×10^7
AF1	2.76	1.0×10^7	1.4×10^7	0.10×10^7

coupling is expected to be smaller than for the d_{xz} and d_{yz} bands. Conversely, its in-plane band width may be expected to be larger, following the number of hopping paths. This qualitatively is what we find.

In Boltzmann theory with the constant scattering time approximation, the conductivity varies as $\sigma_x \sim N(E_F)v_F^2\tau$, where τ is a scattering time. Both the paramagnetic and FM electronic structures are quite anisotropic near E_F as expected from the layered crystal structure. This is also apparent from the Fermi surfaces. The exception is the majority spin in the FM case, which has a low density of states and is 3D in character. This Fermi surface has mixed character due to tilting, but is largely from the bilayer antisymmetric combination of d_{xy} orbitals. Hopping through the CaO rocksalt layers is geometrically allowed by octahedral tilts in this structure, so that even though the Fermi surface has mostly d_{xy} character it involves enough apical O character to produce c -axis dispersion.

Turning to the minority spin channel, in addition to the highly 2D character, there is also significant in plane anisotropy. In the constant scattering time approximation, b direction conductivity is $\sim 50\%$ higher than along a . This means that sample dependent orthorhombic twinning could significantly affect the measured transport and should be considered in interpreting experiments. In plane conduction is dominated by the minority channel and is highly spin polarized²⁸, $P_a^{(2)} = -0.88$ and $P_b^{(2)} = -0.91$. On the other hand, for the FM ordering, while c -axis conductivity is a factor of 20 lower, it has a small opposite polarization, $P_c^{(2)} = +0.19$. The actual value of $P_c^{(2)}$ may actually be somewhat larger, because the multi-sheet minority spin Fermi surface would provide more non-spin-flip scattering channels than the simple majority surface, and so the minority spin scattering time may be shorter than the majority spin. In any case, to our knowledge, this type of direction dependent sign of the polarization is unique to FM $\text{Ca}_3\text{Ru}_2\text{O}_7$. While here it is a scientific curiosity, if found in materials that have true ferromagnetic ground states and large $|P|$ for both directions, it could be of practical importance for sources of spin polarized electrons with spin depending on the contact geometry.

The majority spin Fermi surface consists of a single highly corrugated hole cylinder of mostly d_{xy} charac-

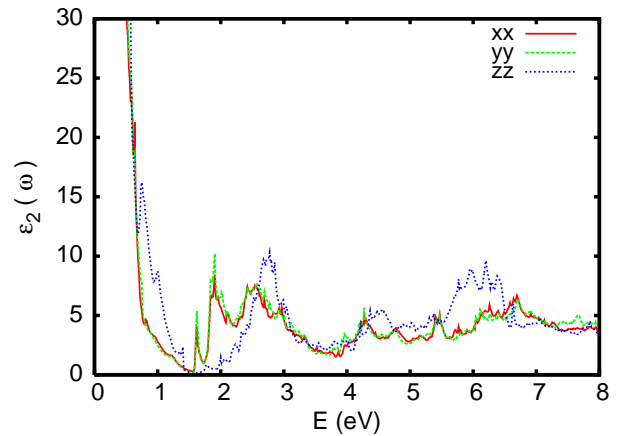


FIG. 3: Optical spectrum (ϵ_2) for FM $\text{Ca}_3\text{Ru}_2\text{O}_7$.

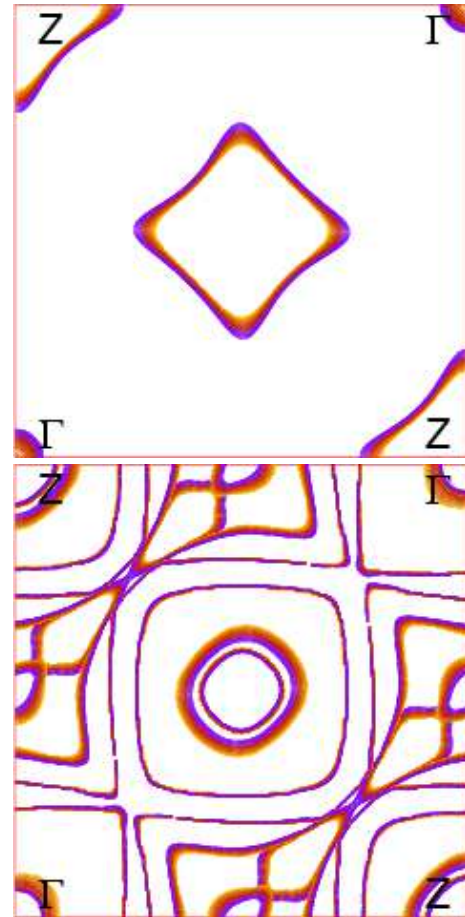


FIG. 4: (color online) Majority (top) and minority (bottom) basal plane extended zone FM Fermi surfaces. The actual zone is half the area and rotated 45° . The plot shows a color map ranging from 1 mRy below E_F (blue) to 1 mRy above (red). The width is inversely proportional to the velocity and electron (hole) surfaces are blue (red) on the interior. The center is a Z point; alternating corners are Γ and Z points due to the centered lattice.

ter around the zone center, which almost pinches off at $k_z = 0$. The minority spin has several sheets of Fermi surface. The highest velocity parts, which contribute most to the in-plane conductivity, are from the symmetric and antisymmetric 1D d_{xz} and d_{yz} sections. These reconnect to form a square cylindrical Γ centered section and an open section, that forms from a square cylinder but opened at the zone boundary at $(1/2,0)$, which is $(1/4,1/4)$ in the extended zone of Fig. 4. Along the other b -direction zone boundary there is a complex set of Fermi surfaces. These derive from the 2D d_{xy} sheets which kiss the zone boundary at $(0,1/2)$. These do not appear along the a direction because the d_{xy} sheet is gapped away by mixing with the 1D d_{xz} and d_{yz} bands due to the octahedral tilts, which are in the a -direction (i.e. around the b -axis). The repulsion from the d_{xz}/d_{yz} Fermi surfaces is strong enough to fold this sheet back in the region around $(1/2,1/2)$ leading to the complex structure seen around this point. The presence of the d_{xy} derived sections towards the b -direction zone boundary, but not the a -direction, is the reason for the large in-plane anisotropy of σ . Besides the major sheets there are two smaller concentric nearly circular cylindrical electron sections around Γ , which are also of substantial d_{xy} character. Significantly, these two minority spin sheets have the same center and are intermediate in size between the maximum and minimum size of the majority spin Fermi surface as a function of k_z . However, they are mis-matched in that the majority surface contains holes and the minority contains electrons.

Turning to the AFM ground state, as mentioned, one might expect the electronic structure of the bi-layers to be essentially unchanged, due to the weak inter-bilayer coupling, and this is confirmed by the calculations. The only notable change is a disruption of the c -axis transport. There are no significant changes²⁹ in $N(E_F)$ or the in-plane $N(E_F)v_F^2$. However, the spin averaged c -axis $N(E_F)v_F^2$ is strongly reduced by a factor of 10 relative to the FM case. This is strong spin-valve physics. Moreover, there is another factor. For non-spin-flip scattering, which ordinarily dominates, there are more scattering channels for the minority spin due to its larger multi-sheet Fermi surface. Thus with AFM stacking, there may be an important change in τ , which would further lower the c -axis conductivity, depending on the relative importance of spin-flip and non-spin-flip scattering, which in turn would depend on details of the sample and temperature.

In summary, we report calculations of the electronic and magnetic properties of $\text{Ca}_3\text{Ru}_2\text{O}_7$, which elucidate the ground state ordering and provide a framework for the strong connections between magnetic order and transport properties, particularly at the metamagnetic transition.

We are grateful for helpful discussions with L. Balicas, M. Braden, G. Cao, S.I. Ikeda, D.G. Mandrus, I.I. Mazin, S. Nagler. We thank Y. Yoshida for a pre-publication copy of Ref. 21. This work was supported by the U.S. Department of Energy.

¹ J.J. Randall and R. Ward, *J. Am. Chem. Soc.* **81**, 2629 (1959).

² A. Kanbayashi, *J. Phys. Soc. Jpn.* **44**, 108 (1978).

³ G. Cao, S. McCall, M. Shepard, J.E. Crow, and R.P. Guertin, *Phys. Rev. B* **56**, 321 (1997).

⁴ Y. Maeno, H. Hashimoto, K. Yoshida, S. Nishizaki, T. Fujita, and J.G. Bednorz, and F. Lichtenberg, *Nature* **372**, 532 (1994).

⁵ S. Nakatsuji, and Y. Maeno, *Phys. Rev. Lett.* **84**, 2666 (2000).

⁶ S.A. Grigera, R.S. Perry, A.J. Schofield, M. Chiao, S.R. Julian, G.G. Lonzarich, S.I. Ikeda, Y. Maeno, A.J. Millis, and A.P. Mackenzie, *Science* **294**, 329 (2001).

⁷ D.J. Singh, *J. Appl. Phys.* **79**, 4818 (1996).

⁸ I.I. Mazin and D.J. Singh, *Phys. Rev. B* **56**, 2556 (1997).

⁹ D.J. Singh and I.I. Mazin, *Phys. Rev. B* **63**, 165101 (2001).

¹⁰ Z. Fang and K. Terakura, *Phys. Rev. B* **64**, 020509(R) (2001).

¹¹ G. Cao, S. McCall, J.E. Crow, and R.P. Guertin, *Phys. Rev. Lett.* **78**, 1751 (1997).

¹² C.S. Snow, S.L. Cooper, G. Cao, J.E. Crow, H. Fukazawa, S. Nakatsuji, and Y. Maeno, *Phys. Rev. Lett.* **89**, 226401 (2002).

¹³ G. Cao, K. Abbound, S. McCall, J.E. Crow, and R.P. Guertin, *Phys. Rev. B* **62**, 998 (2000).

¹⁴ G. Cao, L. Balicas, Y. Xin, E. Dagotto, J.E. Crow, C.S. Nelson, and D.F. Agterberg, *Phys. Rev. B* **67**, 060406 (2003).

¹⁵ G. Cao, L. Balicas, Y. Xin, J.E. Crow, and C.S. Nelson, *Phys. Rev. B* **67**, 184405 (2003).

¹⁶ S. McCall, G. Cao, and J.E. Crow, *Phys. Rev. B* **67**, 094427 (2003).

¹⁷ J.F. Karpus, R. Gupta, H. Barath, and S.L. Cooper, *Phys. Rev. Lett.* **93**, 167205 (2004).

¹⁸ E. Ohmichi, Y. Yoshida, S.I. Ikeda, N. Shirakawa, and T. Osada, *Phys. Rev. B* **70**, 104414 (2004).

¹⁹ G. Cao, L. Balicas, X.N. Lin, S. Chikara, E. Elhami, V. Durairaj, J.W. Brill, R.C. Rai, and J.E. Crow, *Phys. Rev. B* **69**, 014404 (2004).

²⁰ X.N. Lin, Z.X. Zhou, V. Durairaj, P. Schlottmann, and G. Cao, *Phys. Rev. Lett.* **95**, 017203 (2005).

²¹ Y. Yoshida, S.-I. Ikeda, H. Matsuhata, N. Shirakawa, C.H. Lee, and S. Katano, preprint.

²² D.J. Singh, *Planewaves Pseudopotentials and the LAPW Method* (Kluwer Academic, Boston, 1994).

²³ D. Singh, *Phys. Rev. B* **43**, 6388 (1991).

²⁴ Two codes were used. These were the author's LAPW code and WIEN2K. These were cross-checked.

²⁵ P. Blaha, K. Schwarz G.K.H. Madsen, D. Kvasnicka, and J. Luitz, *WIEN2K* (TU Wien, Vienna, 2001).

²⁶ W.E. Pickett and D.J. Singh, *Phys. Rev. B* **53**, 1146 (1996).

²⁷ B. Nadgorny, I.I. Mazin, M. Osofsky, R.J. Soulen, Jr., P. Broussard, R.M. Stroud, D.J. Singh, V.G. Harris, A. Ar

senov and Ya. Mukovskii, Phys. Rev. B **63**, 184433 (2001).

²⁸ I.I. Mazin, Phys. Rev. Lett. **83**, 1427 (1999).

²⁹ The Fermi surface of the doubled ground state AFM supercell was sampled using a lower density \mathbf{k} -point mesh;

the differences for in-plane quantities are at the level of the computational accuracy, and are not significant.